Cold, Electrostatic, Ion-Cyclotron Waves and Ion-Ion Hybrid Resonances

M. Ono

Plasma Physics Laboratory, Princeton University, Princeton, New Jersey 08544

Experimental observation and studies of a new type of cold electrostatic mode near the ion-ion hybrid frequency are presented. The resonance cone behavior associated with this mode is verified. The wave dispersion relation has been measured which shows a clear resonance behavior near the hybrid frequency. Associated with the mode, strong electron Landau damping by bulk electrons and equally strong ion damping near the ion-ion hybrid resonance are observed. This type of mode should be readily excited in high-field devices $(B_0 \gtrsim 30 \text{ kG})$.

Although rf heating near the ion cyclotron frequencies (ICRF) utilizes electromagnetic waves as the principal energy carrier, an important role played by electrostatic waves has been recognized for linear mode-conversion processes occurring near the ion-ion hybrid resonance layer.[1] Since electrostatic waves can be readily absorbed by a plasma, the excitation of such waves would significantly alter the heating efficiencies of such applied rf power. In this report, we present the first experimental observation of what we tentatively call the cold electrostatic ion-cyclotron wave, which turns into a hybrid mode near the ion-ion hybrid resonance. This type of mode can be readily excited in high-field devices $(B_0 \geq 30 \text{ kG})$ with hydrogen (and D-T as well) plasmas.

The real part of the wave dispersion relation is written in the following form[2]:

$$1 + [1 + yZ(y)]\frac{\omega_{pe}^2}{k^2}\frac{m_e}{T_e} + \sum_\sigma \frac{\omega_{p\sigma}^2}{\Omega_\sigma^2 - \omega^2}\frac{k_\perp^2}{k^2} = 0, \quad (1)$$

where $y = \omega/k_\parallel \cdot (m_e/2T_e)^{1/2}$, Z is the plasma dispersion function,[3] and σ designates all species. In deriving Eq. (1), we let $(V_i k_\parallel/\omega)^2$, $(k_\parallel/k_\perp)^2 = O(m_e/m_i)$, and $(k_\perp \rho_\sigma)^2$ be small. For simplicity, we now let the electrons be cold [a reasonable approximation for $\omega/k_\parallel V_e \geq 1.5$, where $V_e = (T_e/m_e)^{1/2}$] and the plasma to have two types of ions. Then Eq. (1) can be written as follows:

$$1 - \frac{\omega_{pe}^2}{\omega^2}\frac{k_\parallel^2}{k^2}$$

$$+ \frac{(\omega_{p1}^2 + \omega_{p2}^2)(\omega^2 - \omega_{IH}^2)}{(\omega^2 - \Omega_1^2)(\Omega_2^2 - \omega^2)}\frac{k_\perp}{k^2} + \frac{\omega_{pe}^2}{\Omega_e^2}\frac{k_\perp^2}{k^2} = 0, \quad (2)$$

where $\Omega_2 > \Omega_1$ and ω_{IH} is defined as[4]

$$\omega_{IH}^2 = \frac{\omega_{p1}^2\Omega_2^2 + \omega_{p2}^2\Omega_1^2}{\omega_{p1}^2 + \omega_{p2}^2}$$

$$= \Omega_1\Omega_2\left(\frac{N_1 M_1 Z_1 Z_2 + N_2 M_2 Z_1 Z_2}{N_1 M_2 Z_1^2 + N_2 M_1 Z_2^2}\right). \quad (3)$$

Here N_i are the partial ion concentrations and Z_i are their charge states such that $\sum_i N_i Z_i = 1$. The frequency range of wave propagation can be determined from Eq. (2) to be $\omega < \Omega_1$, and $\omega_{res} = \omega_{IH}[1 - O(\Omega_i^2/\Omega_{pi}^2)] < \omega < \Omega_2$. For a given $k_\parallel$, the mode exhibits a resonance below ω_{IH} which depends on the plasma density and cutoffs at Ω_i. For $\omega_{pi} \gg \Omega_i^2$ and ω sufficiently away from ω_{IH}, one can neglect the first and last terms in Eq. (2). Then the dispersion relation becomes independent of plasma density.

We have experimentally investigated this wave in the Princeton L-4 linear research device.[5] The L-4 has a steady-state axial magnetic field of 4.2 kG [$f_{ci}(\text{He}) \simeq 1.6$ MHz] with < 1% field inhomogeneity in an axial length of $\simeq 2.3$ m and a relatively low electron temperature (measured by propagating the ion acoustic wave) of $\simeq 0.5$ eV in the experimental region. Other plasma parameters are as follows: the plasma density $n_0 \simeq (1 - 2) \times 10^{10}$ cm^{-3}; the ion temperature $T_i < 1/10$ eV; and the neutral gas filling pressure $P \simeq 2 \times 10^{-3}$ Torr. In this experiment, helium and neon rather than hydrogen are used since their ion concentration has been previously studied in detail.[5,6]

We first show the so-called "resonance-cone" behavior of the present mode which was first predicted in the work of Fisher and Gould[7] and theoretically investigated in the work of Kuehl.[8] The theory predicts that an electrostatic signal with its Fourier components satisfying the cold plasma condition propagates obliquely into the plasma along a trajectory which makes an angle $\theta = \sin^{-1}(k_\parallel/k)$ with respect to the magnetic field. In Fig. 1(a), a simplified schematic of experimental setup is shown. The resonance-cone–launching structure is essentially a 28-cm-long, $3\frac{1}{2}$-in.-i.d. pipe (actually constructed from nine rings electrically tied together) which is aligned with the axial magnetic field. In the figure, a qualitative picture of the resonance-cone trajectory is shown. The resulting resonance cone is detected by an
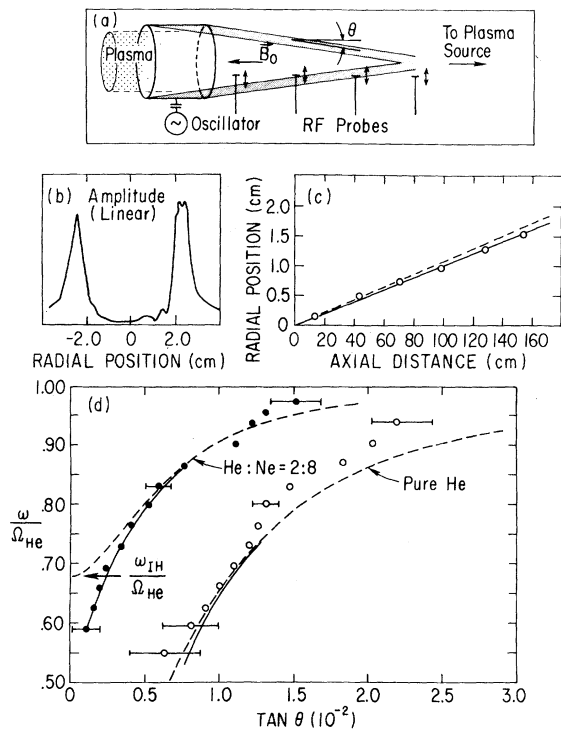
FIG. 1. (a) Simplified schematic of resonance-cone propagation setup. (b) A typical detected radial profile of resonance-cone amplitude. (c) Resonance-cone radial position as a function of axial distance. $f = 1.24$ MHz, $B = 4.1$ kG, He:Ne = 6:4. (d) Resonance-cone angle as a function of ω/Ω_{He} for two ion-concentration ratios (as labeled). The dots are experimental points and curves are that of theory.
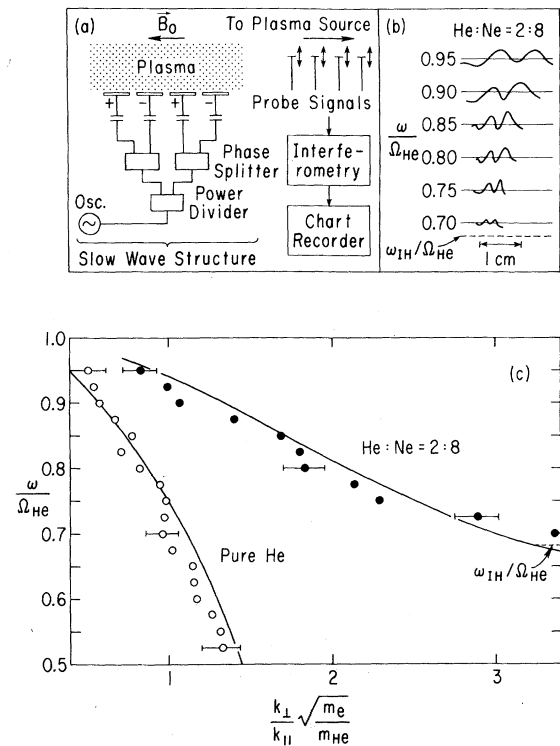
FIG. 2. (a) Simplified schematic of wave propagation setup. (b) Radial interferometry output of propagated wave for various ω/Ω_{He} (as labeled) in He:Ne = 2:8 plasma. (c) Wave dispersion relation for two ion concentrations (as labeled). The dots are experimentally measured values. The solid curves are theoretical values.

array of radially moving rf probes. In Fig. 1(b), a typical radial profile of detected signal is shown. One can measure the resonance-cone angle by plotting the radial position of the amplitude maxima as a function of the axial distance from antenna which is shown in Fig. 1(c). The solid curve is the best-fitted line and the dashed curve is the value computed from Eq. (2) which shows a good agreement.

In Fig. 1(d), the measured cone angles as a function of ω/Ω_{He} are shown for pure helium and He:Ne = 2:8. The dashed curves are computed from Eq. (2) assuming $\omega_{pi}^2/\Omega_i^2 \gg 1$. The agreement is reasonable except near ω_{IH} where the finite-density term becomes important especially since the exciter is located outside of the plasma column where the density is very low. In order to quantitatively account for the density effect, the wave differential equations[9] were solved and the resonance-cone trajectory was calculated including a realistic density profile. The density

profile was measured by the electron plasma-wave resonance-cone propagation[7] which yielded an exponential density profile [i.e., $n(x) = n_0 \times \exp(-x/R)$, where $R \simeq 2$ cm]. This permitted an analytical solution for the trajectory integral and simplified subsequent numerical computations. The result of such a calculation is shown by solid curves in Fig. 1(d). The agreement is now very good even when $\omega \rightarrow \omega_{res} < \omega_{IH}$. Since the above theory, which takes the wave trajectory and the density profile into account, describes our experimental situation quite accurately, the theoretical analysis for the data presented in the following sections were calculated in this manner.

Next, we measured the wave dispersion relation by using a slow-wave structure which excites a mode with fixed $\lambda_{\parallel}$. By fixing $\lambda_{\parallel}$, $\lambda_{\perp}$ is automatically fixed through the wave dispersion relation. It should be noted that this type of behavior has been studied extensively for the lower-hybrid-wave propagation.[10, 11] A simplified schematic of the experimental setup is shown in Fig. 2(a). The present slow-wave structure con-

sists of four identical cylindrical sections where one of the sections was used to excite the resonance cone [see Fig. 1(a)]. The four sections are alternately phased in or out of phase to make two axial wavelengths with $\lambda_{\parallel} \simeq 62$ cm. The half width of the calculated Fourier spectrum is about $\pm 15\%$. The propagation characteristics, the wavelengths and the dampings are measured by a set of radial probes. The measured axial wavelength $\lambda_{\parallel} \simeq 61$ cm is found to stay reasonably constant as expected. The radial wavelength, on the other hand, shows large changes with changes in ion concentrations and ω/Ω_i. In Fig. 2(b), a typical radial interferrogram is shown. From such data, the wavelength can be seen to decrease rapidly as ω approaches $\omega_{IH} \simeq 0.68\Omega_{He}$. The measured dispersion relation is shown in Fig. 2(c) for two concentrations (as marked). The solid curves are theoretically computed values including the finite-electron-temperature effect. The agreement between theory and experiment is seen to be very good.

In this experiment, the waves are propagated with their parallel phase velocities in a range $\omega/k_{\parallel}V_e \simeq 2.0\text{--}3.3$, therefore they can interact with bulk electrons and encounter a strong electron Landau damping. We have measured such damping γ_e as a function of wave phase velocity $\omega/k_{\parallel}$. We define damping rate γ_e such that the wave is damped by $\exp(-\gamma_e)$ as it propagates an axial distance of $\lambda_{\parallel}$. Therefore γ_e can be deduced, for example, from two observation points Z_1 and Z_2 $(Z_1 < Z_2)$ as

$$\gamma_e = \lambda_{\parallel}/(Z_2 - Z_1) \ln[E(Z_1)/E(Z_2)], \qquad (4)$$

where $E(Z_1)$ and $E(Z_2)$ are the measured wave amplitudes at respective positions. In Fig. 3(a), the experimental data points are shown in circles. The measured damping rate increases rapidly as the wave phase velocity is being lowered into the electron thermal distribution [see the inset in Fig. 3(a)]. For $\omega/k_{\parallel}V_e < 2.2$, the wave was attenuated so severely that the measurement could not be done with accuracy. The solid curve in Fig. 3(a) is obtained from theory for a Maxwellian electron distribution with electron-neutral collisions also included.[12] The agreement between theory and experiment appears to be very good. We note that in this experiment the effect of hot primary electrons which are emitted by the tungsten filiment source,[11] is avoided by propagating the wave toward instead of away from the source.

Perhaps the most important phenomenum observed in this experiment is strong ion damping
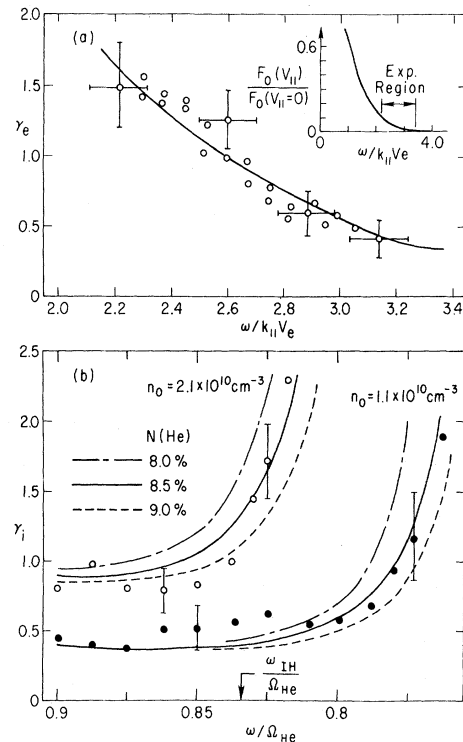

FIG. 3. (a) Wave damping rate due to electron Landau damping and electron-neutral collisions as a function of wave phase velocity. The dots are experimentally measured values and the solid curve is obtained from theory. (b) Wave damping rate due to ion-collisional damping near ion-ion hybrid resonance frequency for two plasma densities (as labeled) in ~8% helium plasma. The dots (solid and circles) are experimentally measured values. The curves are theoretical values for three ion concentrations (as labeled).

associated with the ion-ion hybrid resonance layer. As the wave approaches the resonance, it gradually turns into a pure ion wave whose motion is sustained by a 180° out-of-phase oscillation between ions of different species[4] and the wave group velocities (perpendicular phase velocity as well) slow down considerably. Consequently, near the resonance, a relatively weak collisional process among the two ion species can effectively damp the wave energy, heating bulk ions. In this experiment, we have indeed observed and measured this rapid increase of wave damping as the ion-ion hybrid resonance is approached. The damping was measured with relatively low-helium-concentration plasma thus increasing ω_{res} and minimizing the effect of the electron Landau damping which is subsequently subtracted from the measured damping. In Fig. 3(b), we plot the measured damping rate, γ_i [de-

fined similarly as Eq. (4)], in a He-Ne plasma with 8% helium-ion concentration. The two values of the plasma densities are plotted to show the density dependence of the resonance frequency. We observe ω_{res} approaches ω_{IH} as the density is increased which is in agreement with the theory. As shown by the figure, the measured damping increases rapidly as the wave approaches the resonance frequency. The curves are theoretical values calculated using the experimentally measured parameters. In the calculation, the ion-ion collisions among different ion species (which is the dominant process here) and the ion-neutral collisions are included. The effect of ion viscous damping,[12] $\gamma_i \propto \nu_{ii}(k_\perp \rho_i)^2$ is not included since in this experiment, the wave did not reach the $(k_\perp \rho_i)^2 \sim 1$ regime because of the heavy damping. Since the measured ion concentration has some uncertainties [here $(8 \pm 2)\%$ helium], the calculation was carried out for a range of concentration. From the plot in Fig. 3(b), we see that the best-fitted curve to experimental points is 8.5% helium which is well within the concentration uncertainty, and thus we conclude that the observed damping rate agrees well with theory.

In conclusion, the low-frequency resonance-cone behavior associated with the cold electrostatic ion-cyclotron wave was verified experimentally. With a slow-wave structure, the wave dispersion relation was measured which yielded a strong resonance behavior near the ion-ion hybrid resonance frequency. When $\omega/k_\parallel V_e < 3.0$, the wave was observed to damp heavily by electron

Landau damping. As ω approaches ω_{res}, the wave damping was observed to increase rapidly due to the ion-ion collisions. Throughout the experiment, the measured values were found to agree well with theory.

[1]F. W. Perkins, Nucl. Fusion 17, 1197. This also gives references to earlier work.

[2]T. H. Stix, Theory of Plasma Waves (McGraw-Hill, New York, 1962).

[3]B. D. Fried and S. D. Conte, The Plasma Dispersion Function (Academic, New York, 1961).

[4]S. J. Buchsbaum, Phys. Fluids 3, 418 (1960).

[5]M. Ono, R. P. H. Chang, and M. Porkolab, Phys. Rev. Lett. 38, 962 (1977).

[6]M. Ono, Ph.D. thesis, Princeton University, 1978 (unpublished).

[7]P. K. Fisher and R. W. Gould, Phys. Fluids 14, 857 (1971).

[8]H. H. Kuehl, Phys. Fluids 17, 1636 (1974).

[9]R. J. Briggs and R. R. Parker, Phys. Rev. Lett. 29, 852 (1972).

[10]P. M. Bellan and M. Porkolab, Phys. Rev. Lett. 34, 124 (1975).

[11]P. M. Bellan and M. Porkolab, Phys. Fluids 17, 1592 (1974), and 19, 995 (1976).

[12]M. Porkolab, Phys. Fluids 11, 834 (1968).

Small-Scale Magnetic Fluctuations Inside the Macrotor Tokamak

S. J. Zweben, C. R. Menyuk, and R. J. Taylor

Center for Plasma Physics and Fusion Engineering, University of California, Los Angeles, California 90024

(Received 15 January 1979)

Magnetic pickup loops inserted into the Macrotor tokamak have shown a broad spectrum of oscillation in B_r and B_θ up to $f \approx 100$ kHz. The high-frequency $\tilde{B}_r$ have short radial and poloidal correlation lengths $L < 5$ cm, in contrast with the usual Mirnov oscillations with $f \approx 7$ kHz and $L \gg 5$ cm. The observed magnitude $\Sigma |\tilde{B}_r|/B_T > 10^{-5}$, where the summation extends over all $f > 30$ kHz, is in the range in which such radial magnetic perturbations may be contributing to anomalous electron energy transport.

The persistent anomaly of electron energy confinement in tokamaks has recently stimulated discussion of magnetic-fluctuation–induced transport.[1-4] In this Letter we describe what we believe are the first observations of small-scale

radial magnetic fluctuations inside a tokamak plasma. Such fluctuations can in theory cause enhanced radial energy flow through a local restructuring or destruction of the magnetic flux surfaces.